

4 THERMALLY PERTURBED SEEPAGE—REFLUX 3

Indications of thermal refluxing have been documented during heater tests performed at the laboratory scale (Green and Prikryl, 1998), small field scale (Lin, et al., 2001), and large field scale (Bechtel SAIC Company, LLC, 2002). These indications were in the form of temperature excursions, corrosion of the engineered barrier system materials, and dripping into air voids [Table 4-1]. In-situ heater tests were not typically designed to observe these indications of thermal refluxing.

In the thermal period as pore water near the drift wall vaporizes, migrates, and condenses at relatively cooler regions outside the boiling isotherm away from the drift wall, a dryout zone is formed between the drift wall and the boiling isotherm. The water volume above the boiling isotherm is also supplemented by deep percolating water in the thermal period, after its flux rate is modified by the mountain-scale and drift-scale seepage factors (Figure 2-2). Hence, the volume of water above the boiling isotherm increases as deep percolation continues. The condensed water above the boiling isotherm can breach the dryout zone during the thermal period if its potential penetration length exceeds the dryout zone thickness. The penetration of the condensed water can be computed as a function of volumetric flow rate above the boiling isotherm using the modified O.M. Phillips equation (Phillips, 1996).

$$L = \sqrt{\frac{q_{perc} h \rho_w}{k \nabla T}} \quad (4-1)$$

where

L	—	penetration length [m]
q_{perc}	—	volumetric flow rate above the dryout zone [m ³ /yr] (Figure 2-1)
h	—	latent heat of evaporation [J/kg] (EnthalpyOfPhaseChangeForWater [J/kg] in tpa.inp)
ρ_w	—	density of boiling water [kg/m ³] (DensityOfWaterAtBoiling[kg/m ³] in tpa.inp)
k	—	thermal conductivity of the host rock [W/(m-K)] (ThermalConductivityOfYMRock [W/(m-K)] in tpa.inp)
∇T	—	temperature gradient near the boiling isotherm [K/m] (TemperatureGradientInVicinityofBoilingIsotherm [K/m] in tpa.inp)

Implementation in TPA Version 5.1

In (TPA) Version 5.1, the EnthalpyOfPhaseChangeforWater[J/kg] is 2.67×10^6 J/kg [1.15×10^3 BTU/lb] and the DensityOfWaterAtBoiling[kg/m³] is 961 kg/m³ [60 lb/ft³]. Thermal conductivity ofYMRock [W/(m-K)] is sampled from a uniform distribution in the range of 1.90–2.30 W/(m-K) [1.1–1.3 BTU/(hr-ft-°F)]. The TemperatureGradientInVicinityof BoilingIsotherm [K/m] is sampled from a uniform distribution in the range of 1–20 K/m [0.54–10.8 °R/ft]. Transient volumetric flow rate, q_{perc} , is computed in TPA Version 5.1 based on the mass balance equation for water flux. If the computed penetration depth exceeds the sampled dryout zone thickness, q_{perc} breaches the dryout zone during the thermal period. A time series of the dryout thickness was computed externally using a process-level model (Manepally, et al., 2004) for both degraded and intact drift scenarios, and the results are stored in an auxiliary input file drythick.dat.

Table 4-1. Direct and Indirect Observations for Thermal Seepage		
Date	Test	Evidence
1977–1978	Climax Small Borehole Test, Nevada Test Site, Nevada	Temperature excursion*
1980–1983	Climax Spent Fuel Test, Nevada Test Site, Nevada	Dripping onto heater †
1980–1984	Sandia National Laboratory G-Tunnel heater tests, Nevada Test Site, Nevada	Temperature excursion‡ §
1988–1989	Lawrence Livermore National Laboratory, G-Tunnel heater test, Nevada Test Site, Nevada	Corrosive fluid buildup on resonator
1994–1995	Large Block Test, Fran Ridge, Nevada	Episodic dripping (temperature)¶
1996–1997	Single Heater Test	Solute staining on fracture surfaces consistent with evaporated reflux water and corrosion of engineered materials #
1997–2005	Drift Scale Test, Exploratory Studies Facility, Nevada	Dripping into heated drift, temperature excursions and corrosion of engineered materials**
1996–1997	CNWRA Laboratory Scale tests	Dripping into drift, temperature excursions and corrosion of engineered materials ††

*Montan, D.N. and W.E. Bradkin. "Heater Test 1, Climax Stock Granite, Nevada." UCRL-53496. Livermore, California: Lawrence Livermore National Laboratory. 20p + appendices. 1984.

†Patrick, W. "Spent Fuel Test–Climax: An Evaluation Of The Technical Feasibility Of Geologic Storage Of Spent Nuclear Fuel In Granite. Final Report." UCRL-53702. Livermore, California: Lawrence Livermore National Laboratory. 297p. 1986.

‡Zimmerman, R.M., M.L. Blanford, J.F. Holland, R.L. Schuch, and W. Barrett. "Final Report: G-Tunnel Small-Diameter Heater Experiments." SNL SAND84-2621, DE87-007361. Albuquerque, New Mexico: Sandia National Laboratories. December 1986.

§Zimmerman, R.M., R.L. Schuch, D.S. Mason, M.L. Wilson, M.E. Hall, M.P. Board, R.P. Bellman, and M.P. Blanford. "Final Report: G-Tunnel Heated Block Experiment." SNL SAND84-2620, DE86-011768 Albuquerque, New Mexico: Sandia National Laboratories. April 1986.

||Ramirez, A.L. "Prototype Engineered Barrier System Field Tests (PEBSFT). Final Report." UCID-106159. Livermore, California: Lawrence Livermore National Laboratory. 1991.

¶Lin, W., S.C. Blair, D. Wilder, S. Carlson, J. Wagoner, L. DeLoach, G. Danko, A.L. Ramirez, and K. Lee. "Large Block Test Final Report." UCRL-ID-132246, Rev. 2. TIC 252918. Livermore, California: Lawrence Livermore National Laboratory. 2001.

#CRWMS M&O. "Single Heater Test Final Report." BAB000000-01717-5700-00005 Rev. 00 ICN 01. Las Vegas, Nevada: CRWMS M&O. ACC: MOL.20000103.0634. 129261. Bechtel SAIC Company. CRWMS M&O. 1999.

**Bechtel SAIC Company, LLC. "Thermal Testing Measurements Report." ANL-NBS-HS-000041. ACC: MOL.20021004.0314. Rev 00. Las Vegas, Nevada: Bechtel SAIC Company. LLC. 2002.

††Green, R.T. and J.D. Prikryl. "Formation Of A Dry-out Zone Around A Heat Source In A Fractured Porous Medium." Proceedings for the Second International Symposium on Two-Phase Flow Modeling and Experimentation. May 23–26, 1999. Pisa, Italy. Edizioni ETS. 1999.

In Eq. (4-1), the TemperatureGradientInVicinityOfBoilingIsotherm [K/m], ∇T (representative for the dryout zone), is not explicitly linked to the actual temperature at the drift wall or across the dryout zone. In the beginning of the thermal period, if the lower bound is sampled for ∇T , the computed penetration depth, L , will be a large number. In this case, when q_{perc} is high, k is at its upper bound, ∇T is at its lower bound, and the dryout zone can be breached even at high drift wall temperatures, which might be unrealistic. To eliminate unrealistic cases, a factor called SeepageThresholdT[C] is introduced in TPA Version 5.1. For the intact drift scenario, if the drift wall temperature remains above the SeepageThresholdT[C], the dryout zone is not breached, even if the penetration depth of the condensed water exceeds the dryout zone thickness. Similarly, for the degraded drift scenario, the flux across the dryout zone may occur only if the drip shield temperature cools down below the SeepageThresholdT[C]. In TPA Version 5.1, SeepageThresholdT[C] is sampled from a triangular distribution with a lower bound, mode, and upper bound of 100, 105, 125 °C [212, 221 and 257 °F], based on an assessment of heater test anecdotal evidence. Indications of thermal refluxing were observed in borehole MPBX-9 of the Drift-scale heat test. Refluxing water, which originated at the boiling isotherm located over 10m [32.81 ft] above the drift crown, dripped down the open boreholes as far as the drift crown. In this case, thermal refluxing penetrated about 10 m [32.81 ft] of boiling rock to a point where the rock temperature was approximately 200°C [392°F] (Bechtel SAIC Company, LLC, 2002).

5 EXPLORATORY QUANTITATIVE ANALYSES

Exploratory analyses considering alternative models were performed for seepage threshold, and amount of evaporated and condensed water that returns to the drip shield or waste package footprint. These exploratory analyses shed light on the complexities of processes in the near-field, and thus are presented here even though these models have not been abstracted for inclusion into TPA 5.1.

5.1 An Alternative Approach for Calculating the Temperature Gradient

As discussed in Section 4, SeepageThresholdT[C] is introduced in TPA Version 5.1 to prevent water from breaching through the dryout zone at high drift wall or drip shield temperatures. An alternative approach for reflux calculations without using SeepageThresholdT[C] is examined in this section.

Noting that the O.M. Phillips equation (Equation 4-1) only uses temperature gradient, and that temperature gradients at different temperatures may affect the amount of water breaching the dryout zone, the alternative model illustrates a possible approach for correlating temperature gradient with temperature at the drift wall. In addition, the temperature gradient in Equation 4-1 should be representative of the entire dryout zone.

Figure 5-1 shows the temperature gradients calculated at different locations along the dryout zone at different times. The temperatures and their gradients were estimated with a drift-scale thermohydrological simulations using MULTIFLO™ (Lichtner and Seth, 1996; Painter, et al., 2001). The leftmost point of every line in Figure 5-1 is at the outermost edge of the dryout zone, and the rightmost point is at the drift crown. This illustrates that the temperature gradient is small near the boiling isotherm and increases toward the drift wall. Thus, estimating a representative temperature gradient for the O.M. Phillips equation (Phillips, 1996) is not straightforward. Also, the temperature gradients are much higher before the peak temperature is reached, as compared to afterward when the temperatures are decaying.

Spatial averages of simulated temperature gradients in the dryout zone at any particularly time are plotted in Figure 5-2 against the corresponding drift wall temperature. The average temperature gradient across the entire dryout zone is intended to reflect the representative temperature gradient in the O.M. Phillips equation (Phillips, 1996). The simulated results in Figure 5-2 can be empirically fitted to the exponential relation:

$$\nabla T = \nabla T_{P0} + ae^{bT} \quad (5-1)$$

where

a	—	0.0000254 °C /m [0.000013935 °F/ft] with vapor pressure lowering
	—	0.0000236 °C /m [0.000012947 °F/ft] without vapor pressure lowering
b	—	0.084 1/°C [0.0187 1/°F] with vapor pressure lowering
	—	0.0699 1/°C [0.0173 1/°F] without vapor pressure lowering
∇T_{P0}	—	1.1757 °C /m [0.645036 °F/ft] with vapor pressure lowering
	—	1.290 °C /m [0.7077456 °F/ft] without vapor pressure lowering
T	—	Rock temperature [°C]

In Eq. (5-1), a, b, and ∇T_{P0} are curve-fitting parameters to be derived from the process-level simulations. The temperature gradient, ∇T_{P0} , is the simulated point value at different locations in the dryout zone. Interfacial forces alter the bulk properties and thermodynamics of water. The effects of capillarity and dissolved species on water properties are both known, however, only the effect of capillarity was incorporated for the simulation results shown in Figure 5-2. Inclusion of the effect of capillarity on water properties is labeled as the vapor-phase lowering case. In process-level simulations using MULTIFLO™, the capillarity effect is accounted for through the use of the Kelvin equation.

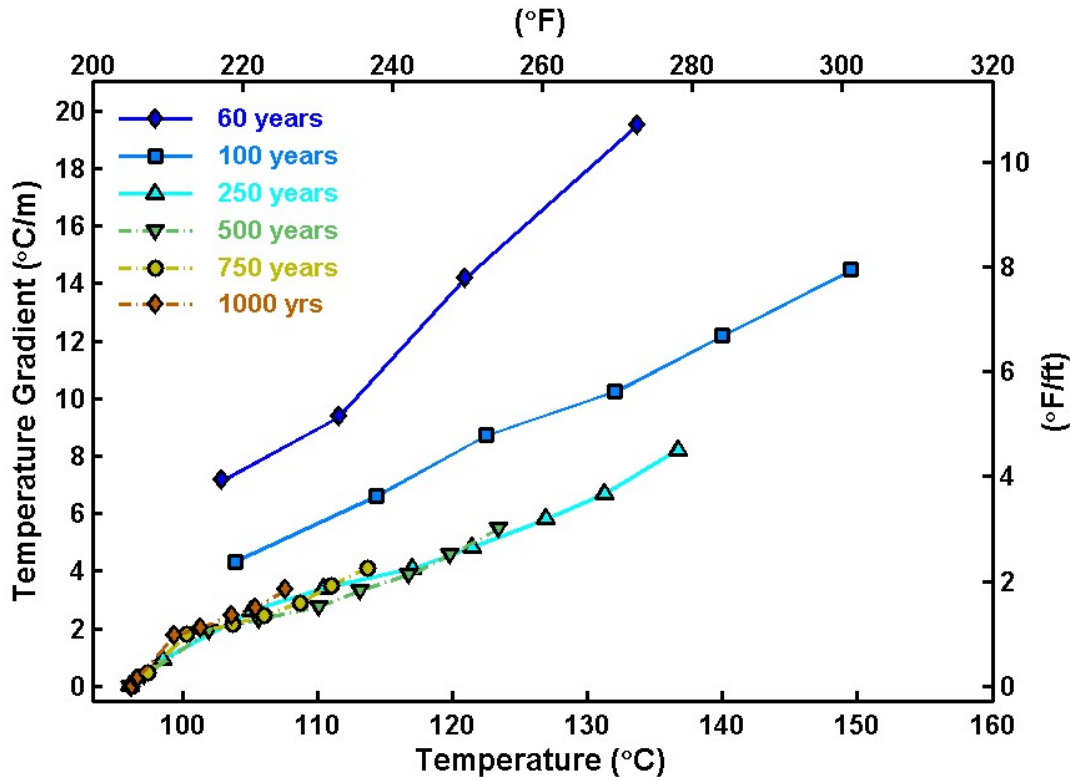


Figure 5-1. Temperature Gradient at Different Locations at Different Times

5.2 Radial Vapor Transport in the Rubble Zone

This section presents an exploratory analysis for quantifying the significance of vapor flow across the rubble in a degraded drift. There is a period when the drift wall temperature may be below the boiling temperature, but the drip shield and waste package temperatures may be above the boiling temperature. During this period, water that seeps through the rubble can vaporize as it gets closer to the waste package; the vapor may migrate outward because of

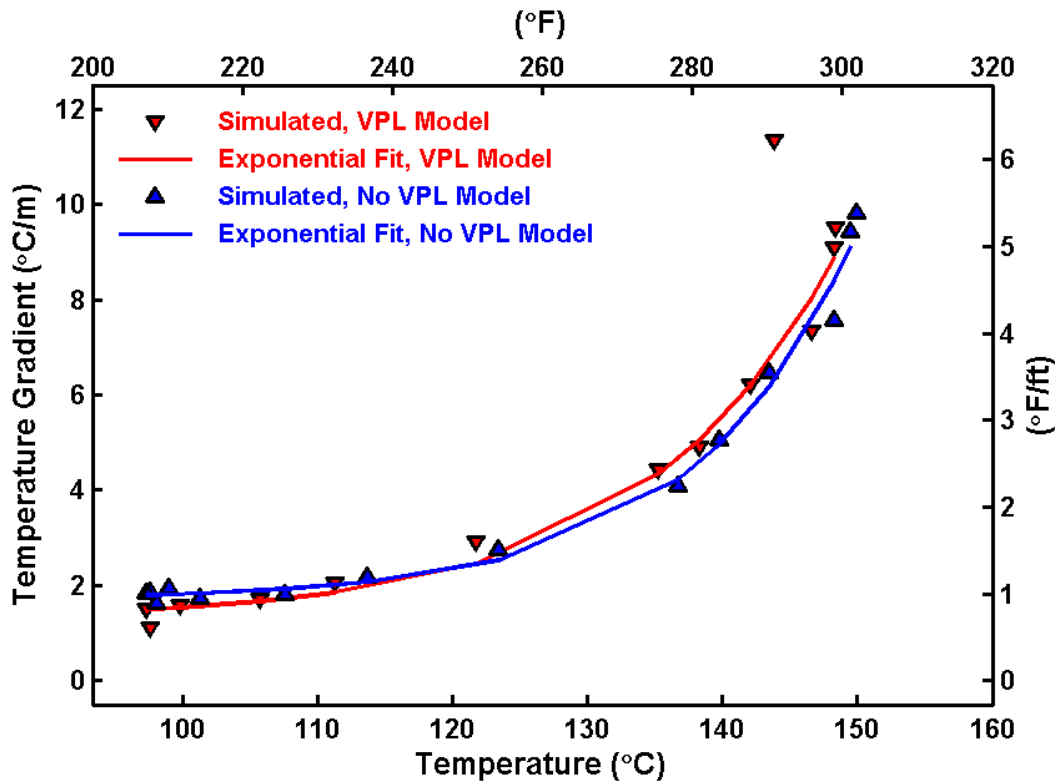


Figure 5-2. Simulated Spatially Averaged Temperature Gradient and Drift Wall Temperature With Vapor Pressure Lowering (VPL in the Legend) and Without Vapor Pressure Lowering (No VPL in the Legend) for Postpeak Temperatures.

vapor concentration gradients and condenses at cooler regions away from the heat source as shown schematically in Figure 5.3. As the water in vapor form reaches cooler regions, it condenses and flows downwards under gravity. The evaporation- condensation cycle could potentially remove some water that otherwise might contact the EBS after the thermal period. Preliminary quantitative analyses were conducted to test the significance of removal of evaporation–condensation cycle-driven water sources in the rubble zone.

In the analyses, vaporized water is assumed to be transported radially away from the heat source and condense at relatively cooler sites. In the meantime, the condensed water at cooler sites vertically flows downward to relatively warmer sites under gravity (the effects of capillary flow in the rubble are neglected). This cycle continues as long as the temperature and density gradients between the EBS components and the drift wall exist. The process is schematically shown in Figure 5-3.

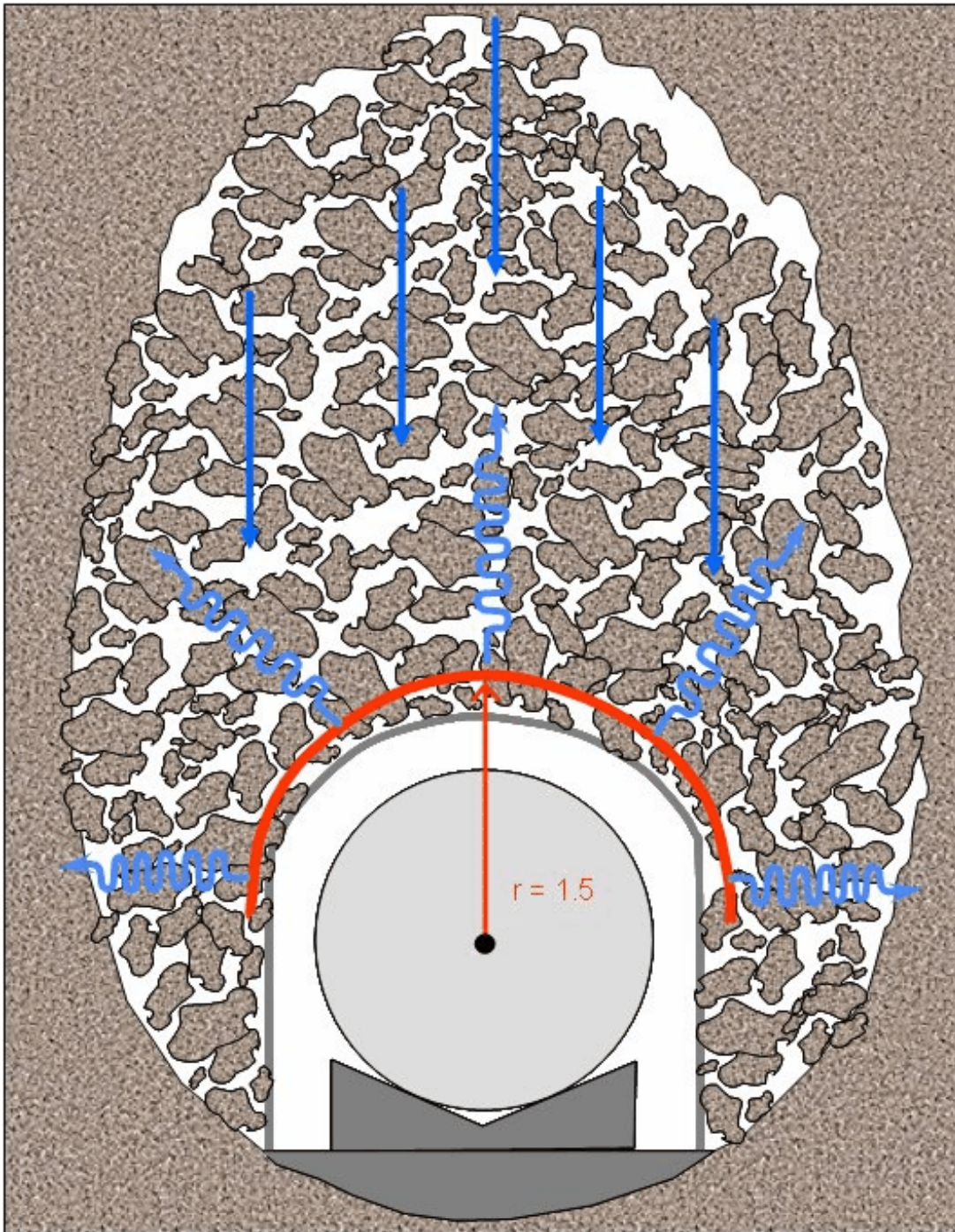


Figure 5-3. A Schematic View of the Flow of Vaporized Water (Spiral Lines) and Condensed Water (Straight Lines) in a Degraded Drift

5.2.1 Assumptions

There are two fundamental assumptions of this analysis: (i) vaporized water transports only in the radial direction (i.e. convection and buoyancy are assumed negligible) and (ii) liquid water only moves vertically down due to gravity. Additional assumptions include:

- Water can condense on the top of the rubble pile or at the interfaces between the rubble and rock wall and the rubble and the air.
- The relative humidity near the waste package is approximately 100 percent.
- The rubble zone is a continuum that allows both evaporation and condensation to occur.
- The temperatures of the domain are not significantly affected by the condensation or evaporation process.
- The rubble surface temperature and the drift wall temperatures are equal.

5.2.2 Conceptualization and Formulation

The analysis was carried out to quantify the amount of water that could be removed in the rubble zone due to the evaporation–condensation process and would not be available to contact the EBS after the thermal period. The conceptual model used for the quantitative analysis is shown in Figure 5-4.

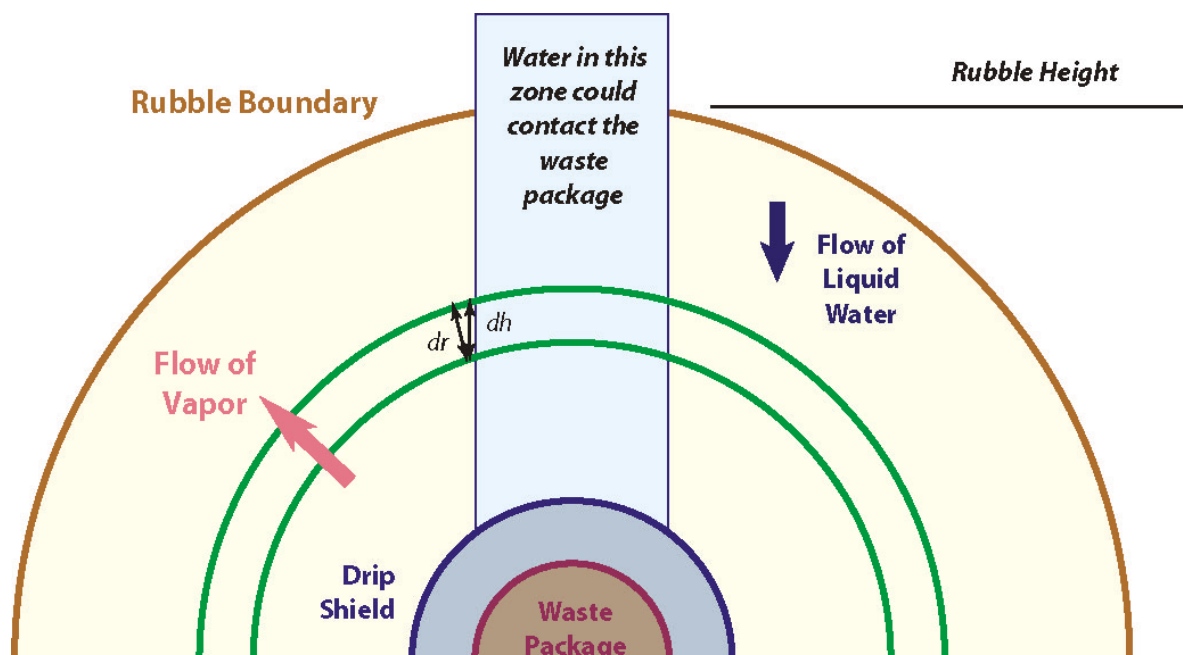


Figure 5-4. Conceptual Model for the Radial Transport Problem. The Symbols dr and dh Are the Incremental Radial and Vertical Distances.

The flow domain between the drip shield and drift wall was represented as a series of porous concentric semicircular surfaces that allow vapor flow throughout and condensation only on

outer surfaces. The flow direction of vaporized and condensed water is shown with pink and blue arrows respectively in Figure 5-4. As mentioned before, the liquid water moves vertically downwards under gravity while vapor radially moves away from the thermal source.

For the temperature range of 50–80 °C [122–176 °F], the saturated water vapor pressure was calculated as a function of temperature using the correlation by Keenan, et al. (1969). Water vapor density in the flow domain bounded by the waste package and the drift wall was calculated based on the ideal gas law and using the saturated vapor pressure and surface temperature.

Liquid water that resides in the blue shaded area vertically above the waste package in Figure 5-4 may flow downward and eventually contact the EBS. Liquid water droplets at any other location outside the shaded region presumably would not contact the waste package during their downward migration. Any water vapor that leaves the blue shaded region would result in removal of a fraction of water that might have flowed downward to contact the EBS. From the mathematical standpoint (Bird, et al., 1960), the analysis should provide insights into how much vapor is transported away along the vertical line of length “dh” in Figure 5-4.

5.2.3 Governing Equations

The governing equations for temperature and vapor flux in a radial coordinate system are

$$\frac{1}{r} \frac{d}{dr} \left(kr \frac{dT}{dr} \right) = 0 \quad (5-2)$$

$$r \frac{dN}{dr} + N = 0 \quad (5-3)$$

$$N = \frac{-\rho D}{1 - \omega_w} \frac{d\omega_w}{dr} \quad (5-4)$$

where

k	—	thermal conductivity of rubble [J/(kg·°C)]
T	—	radial temperature [K]
N	—	radial vapor flux [kg/m ²]
r	—	radial distance [m]
ρ	—	total density of air and water vapor [kg/m ³]
D	—	molecular diffusion coefficient [m ² /s]
ω_w	—	water vapor mass fraction [dimensionless]

Equation (5-2) defines the temperature field, and Eqs. (5-3) and (5-4) define the vapor flux process. The drift wall temperature was fixed at 20°C [68°F]. The drip shield temperature varies between 40°C [104°F] and 120°C [248°F]. For the flux equation, the saturated vapor condition corresponding to any temperature was used as a boundary condition. The following constitutive relations were used to determine the saturation pressure (Keenan, et al., 1969):

$$\log_{10}\left(\frac{P_{vsat}}{218.167}\right) = -\frac{\beta}{T}\left(\frac{a + b\beta + c\beta^2}{1 + d\beta}\right) \quad (5-5)$$

where

P_{vsat}	—	pressure corresponding to saturation temperature [Pa]
β	—	$(647.27 - T)$ [K]
a	—	3.2437814 [dimensionless]
b	—	5.86276×10^{-3} [K ⁻¹]
c	—	1.1702379×10^{-8} [K ⁻²]
d	—	2.1878462×10^{-3} [K ⁻¹]

Two sets of numerical analyses were performed. In the first set of analyses, the rubble height was varied at a fixed temperature difference between the drip shield and the drift wall. In the second set of analyses, the rubble thickness remained constant and the temperature difference across the rubble was varied.

5.2.4 Results

Figure 5-5 shows spatial variations in the water flux removed from the system due to evaporation for different rubble thicknesses. Figure 5-5 shows that for the same temperature gradient, the amount of water removed due to evaporation decreases with an increased rubble thickness. When the temperature difference between the waste package and the drift wall is fixed, an increased rubble thickness reduces the temperature gradient and hence the quantity of transported water vapor also decreases.

Figure 5-6 shows the water flux removed from the system due to changes in the temperature difference for a fixed rubble thickness. As the temperature difference increases, the quantity of transported water increases. For a fixed rubble thickness, the temperature gradient is proportional to the temperature difference between the drift wall and the drip shield. As the temperature gradient increases, the radially transported volume of water away from the thermal source also increases.

Figure 5-7 shows the comparison of the flux rate of condensed water that vertically flowed downward (only along the shaded region) toward the drip shield and the quantity of water vapor transported away from the thermal source for different waste package temperature with time. The temperature difference between the waste package and the drift wall in this case does not exceed 45°C. The space between the drip shield and the drift wall is filled with rubble. Only a fraction of water evaporated and moved out of the system even when the temperature gradient was relatively high. Hence, the vapor transport process alone will not be able to keep the drip shield dry.

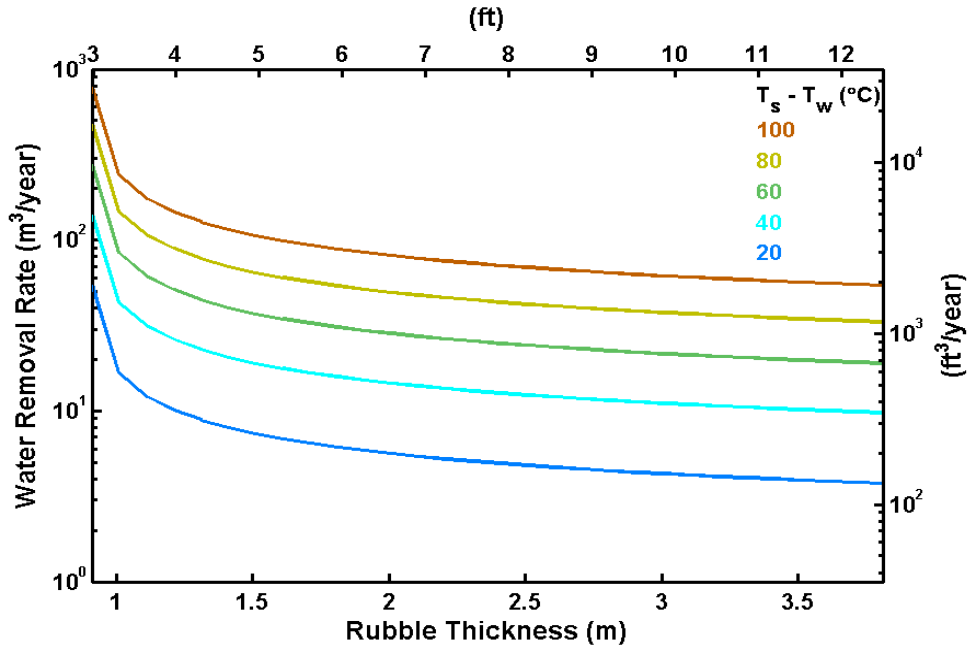


Figure 5-5. Variations in Water Removal Rate as a Function of Changes in Rubble Thickness and Temperature Difference Across the Rubble.

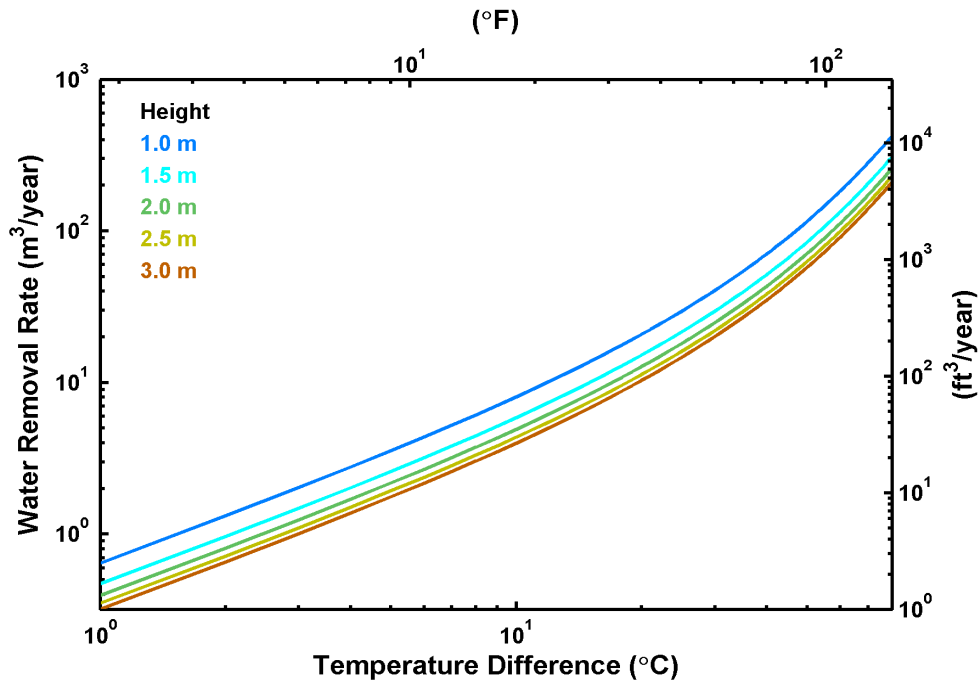


Figure 5-6. Variations in Water Removal Rate as a Function of Changes in Temperature Difference Between the Drip Shield and the Drift Wall and Rubble Thickness.

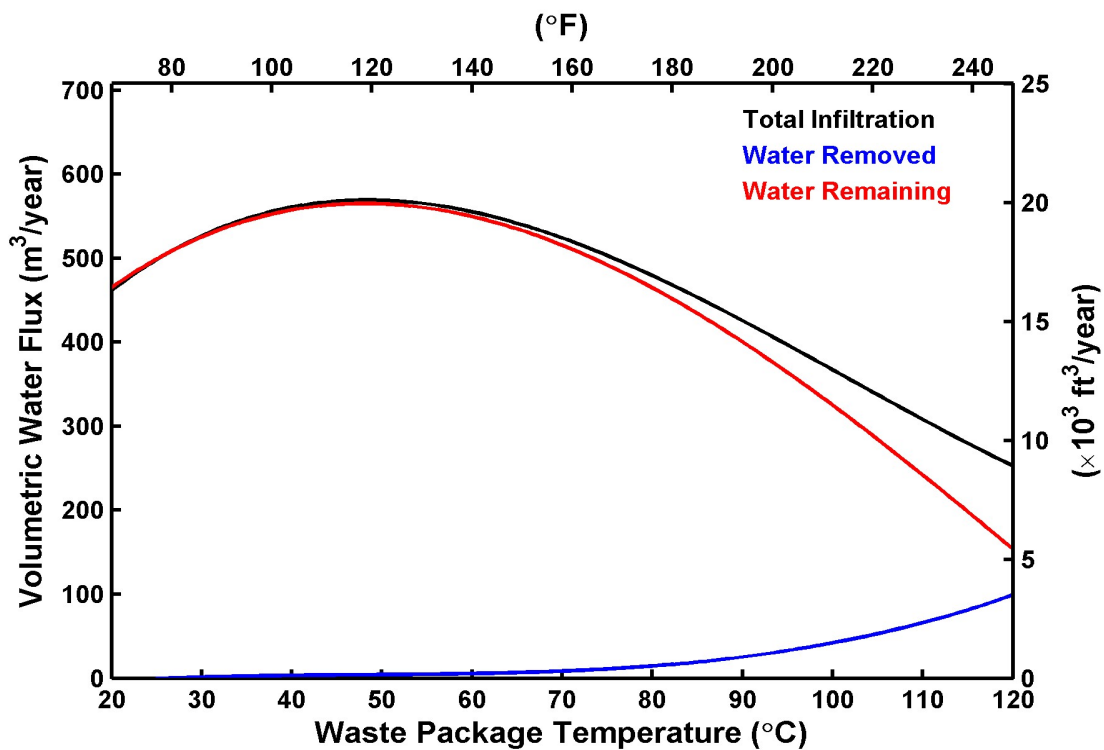


Figure 5-7. Variations in Water Removal Rate Due to Change in Temperature Difference Between the Drip Shield and the Drift Wall.

5.3 Convective Axial Vapor Flow in the Rubble Zone

This section presents the exploratory analysis performed to quantify the mass of water that could be evaporated due to axial convection along the drift when there is liquid water present on the waste package surface. A temperature gradient exists in the axial direction of the drift due to an uneven heat load along a drift caused by variations in spent fuel characteristics, the presence of in-drift components and edge cooling. This temperature gradient creates a natural convection which may evaporate liquid water that may have dripped onto waste packages and transport it to relatively cold surfaces where it condenses. This condensation is known as cold trap process. For the occurrence of condensation, the surface temperature has to be below boiling temperature which for the elevation of the potential repository horizon is nominally 96 °C [205 °F]. In the present calculation, an analytical study was carried out to estimate the quantity of water that would be evaporated due to the axial flow of vapor.

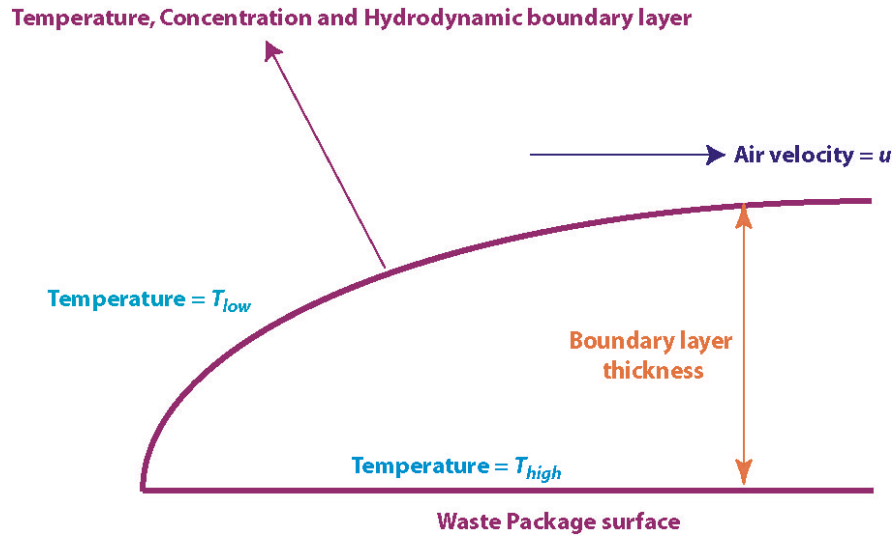


Figure 5-8. A Schematic Representation of a Boundary Layer Problem for Vapor Transport Due to Convective Axial Flow

5.3.1 Assumptions

A boundary layer approach was adopted for this analysis. The schematic is given in Figure 5-8. The basic assumptions are (i) liquid water is available on the waste package surface, (ii) hydrodynamic and concentration boundary layers coincide (this is valid for the present scenario where the Schmidt number is approximately 0.9, which implies that momentum diffusivity and molecular diffusivity are nearly equal), (iii) thermal and hydrodynamic boundary layers coincide (this assumption is valid for the present scenario where the Prandtl number is approximately 0.75, which implies that momentum diffusivity and thermal diffusivity are nearly equal), (iv) the boundary layer is turbulent and (v) the boundary layer is not affected by the presence of rubble in the drift.

5.3.2 Conceptualization and Formulation

The process of vapor transport due to convective axial flow was conceptualized as a boundary layer problem over a presumably planar waste package surface. As shown in Figure 5-8, the growth of the boundary layer starts at the edge of a waste package and continues to grow axially. The velocity is obtained using the 1/7 power law turbulent boundary layer profile (Keenan, et al. 1969). The diffusive vapor flux is obtained using Fick's law, where the vapor density gradient is created by the temperature difference between the waste package and drift wall.

5.3.3 Governing Equations

The mass rate across the boundary layer is calculated using Fick's Law which can be expressed as

$$J = -D \frac{d\rho_w}{dx} \quad (5-6)$$

where

- J — mass flux [kg/(m²-s)]
- D — binary diffusion coefficient [m²/s]
- ρ_w — density of water [kg/m³]
- x — distance along the waste package [m]

Using Equation 5-6 the quantity of water, Q , removed from the waste package surface may be approximated as

$$Q = \int_0^L J dx = \int_0^L D \frac{\rho_{max} - \rho_{min}}{\delta} dx \quad (5-7)$$

where

- L — waste package length [m]
- δ — boundary layer thickness [m]
- ρ_{max} — water vapor density outside the boundary layer [kg/m³]
- ρ_{min} — water vapor density at waste package surface [kg/m³]

The boundary layer thickness, δ , could be derived from the standard 1/7 power law profile for turbulent flows and can be expressed (Fox, et al. 2005) as

$$\delta = \frac{0.382x}{\left(\frac{xu_m}{\nu}\right)^{\frac{1}{5}}} = 0.382x^{\frac{4}{5}} \left(\frac{\nu}{u_m}\right)^{\frac{1}{5}} = C_1 x^{\frac{4}{5}} \quad (5-8)$$

where

- ν — kinematic viscosity [m²/s]
- u_m — mean axial velocity [m/s]

The constant C_1 can be expressed as

$$C_1 = 0.382 \left(\frac{\nu}{u_m}\right)^{\frac{1}{5}} \quad (5-9)$$

Substituting the value of δ from Eq. (5-8) into Eq. (5-7) and integrating the resultant equation for a unit length of the waste package, the quantity of water removed from a waste package surface is

$$\frac{Q}{L} = D \frac{\rho_{max} - \rho_{min}}{5C_1 L^{\frac{4}{5}}} \quad (5-10)$$

5.3.4 Results

By using typical values for the density difference {0.001 to 0.1 kg/m³ [6.242 × 10⁻⁵ to 6.242 × 10⁻³ lb/ft³]}, air velocity {0.01 to 0.1 m/s [0.0328 to 0.328ft/s]}, diffusion coefficient {30 m²/yr [322.92 ft² /yr]}, and kinematic viscosity {1.75 × 10⁻⁵ m²/s [18.531 × 10⁻⁵ ft²/s]}, some typical values of lost water vapor are calculated from Eq. (5-10) and shown in Table 5-1. The results of this exploratory study reveal that a significant quantity of water vapor can potentially be removed by axial convection, but this quantity depends on the temporal variations of the drift environment.

5.4 Condensation and Reflux of Water Above the Dryout Zone

This section describes the exploratory analysis for evaluating the importance of evaporation and condensation processes above the dryout zone during the thermal period. As discussed in Section 4, pore water in the vicinity of the drift wall vaporizes and moves toward the cooler region beyond the boiling isotherm and condenses leaving a dryout zone between the drift wall and the boiling isotherm. The condensed water may reflux across the dryout zone in the thermal period and seep into an emplacement drift (this phenomena is analogous to the evaporation–condensation cycle discussed in connection with radial flow of water vapor in Section 5.2). During the redistribution of water caused by the thermal perturbations, however, a fraction of redistributed water may not be available for refluxing. A preliminary analysis was carried out in this section to quantify this fraction.

Table 5-1. Quantity of Water Evaporated kg/(m-yr) for Different Mean Air Velocity (m/s) and Density (kg/m ³) Differences		
u_m \ $\rho_{max} - \rho_{min}$	0.1	0.01
0.1	2.227	3.52
0.001	0.022	0.0352
1 kg/(yr-m) = 0.67 lb/(yr-ft) 1 m/s = 3.28 ft/s		

5.4.1 Assumptions

Underlying processes and assumptions for water evaporation, transport, and condensation are similar to those discussed in Section 5.2. Vaporized water is assumed to disperse radially away from the thermal source, and liquid water is assumed to migrate vertically downward under gravity.

Other assumptions are

- The mass transfer coefficient used in the analysis is a constant (i.e., treated as a sampled parameter).
- It is a mechanistic model that accounts for the evaporation, condensation and diffusion process, but does not account for hydrological processes associated with the fracture and matrix flows.
- Heat transfer by conduction is assumed between the two radial flow zones.
- The mass-transfer coefficient would depend, for example, on molecular diffusion coefficient, interfacial area between air and water, and tortuosity, and hence it exhibits high degree of uncertainty.

5.4.2 Conceptualization and Formulation

A schematic for the modeling is shown in Figure 5-9. The boiling isotherm is located at R_1 , where the temperature is $100\text{ }^\circ\text{C}$ [$212\text{ }^\circ\text{F}$]. A constant radial vapor flux N_1 is assumed to be present at R_1 . At a distance R_2 , the temperature is assumed to be $20\text{ }^\circ\text{C}$ [$68\text{ }^\circ\text{F}$]. For the present calculation a temperature gradient, and hence a vapor density gradient, exists between R_1 and R_2 ; however, conduction is considered to be the dominant mode of heat transfer. Consider an infinitesimal thickness, dr , in between R_1 and R_2 , as shown in Figure 5-9. As water vapor moves across concentric flow layers, a fraction of it may condense at the layer interface while the rest transports into the next concentric layer. The mass-balance relation yields

$$r \frac{dN}{dr} + N = -rh \frac{d\rho}{dr} \quad (5-11)$$

where

N	—	radial vapor flux [$\text{kg}/(\text{m}^2\text{-yr})$]
r	—	radial distance [m]
ρ	—	total density [kg/m^3]
h	—	mass transfer coefficient [m/s]

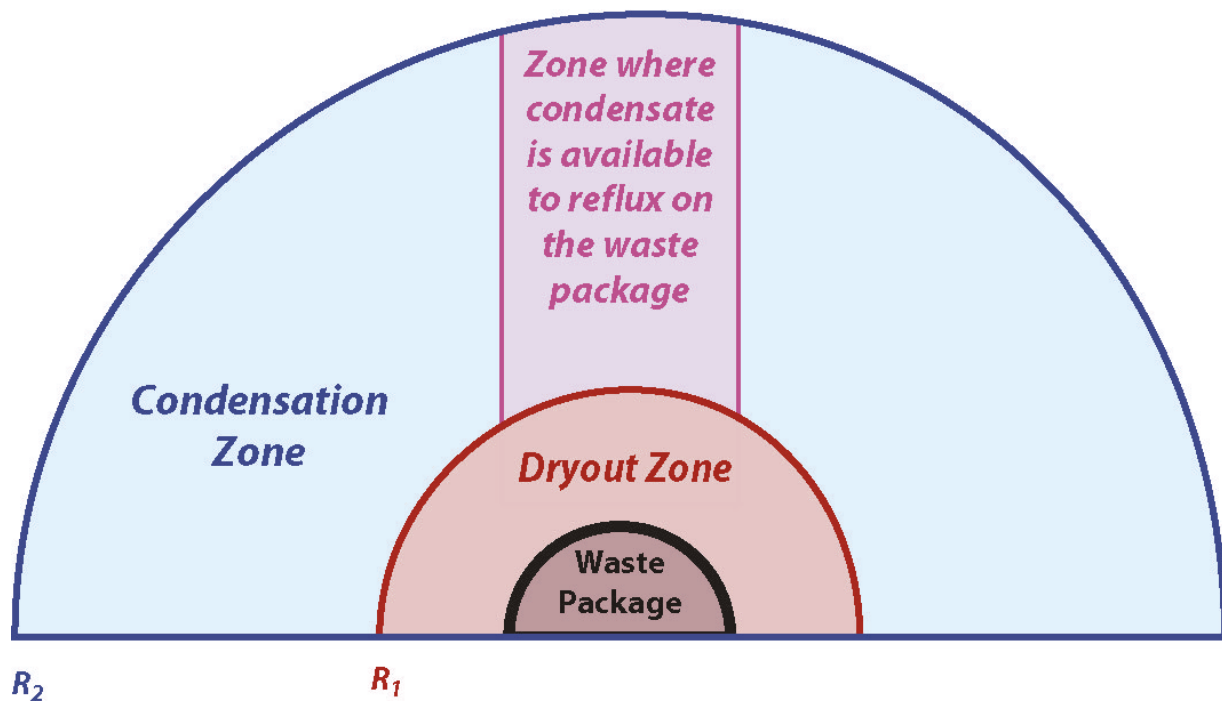


Figure 5-9. Conceptual Model for the Reflux Model

5.4.3. Results

Results are presented in Figures 5-10 and 5-11 for two different dryout zone thicknesses. The minimum dryout zone thickness was assumed to be around 5 m [16.40 ft] and the maximum was about 17 m [55.77 ft]. All the results are presented in terms of nondimensional radial distance $(R - R_1 / R_2 - R_1)$. Figure 5-10 shows the cumulative fraction of condensed liquid water versus the radial distance, from the thermal source for minimum and maximum dryout thickness values respectively. Both curves behaved similarly, but reached the steady values asymptotically at two different radii. Figure 5-11 illustrates the corresponding radial variations of the fraction of water that remains in vapor state. The water vapor content decreased with the radial distance and at a radius of 0.1–0.15, only 10 percent of vapor remained in the system. It is estimated that about 1.6–5 percent of the evaporated water will later reflux back depending on the dryout zone thickness, which would likely affect the total volume of water available for breaching the dryout zone.

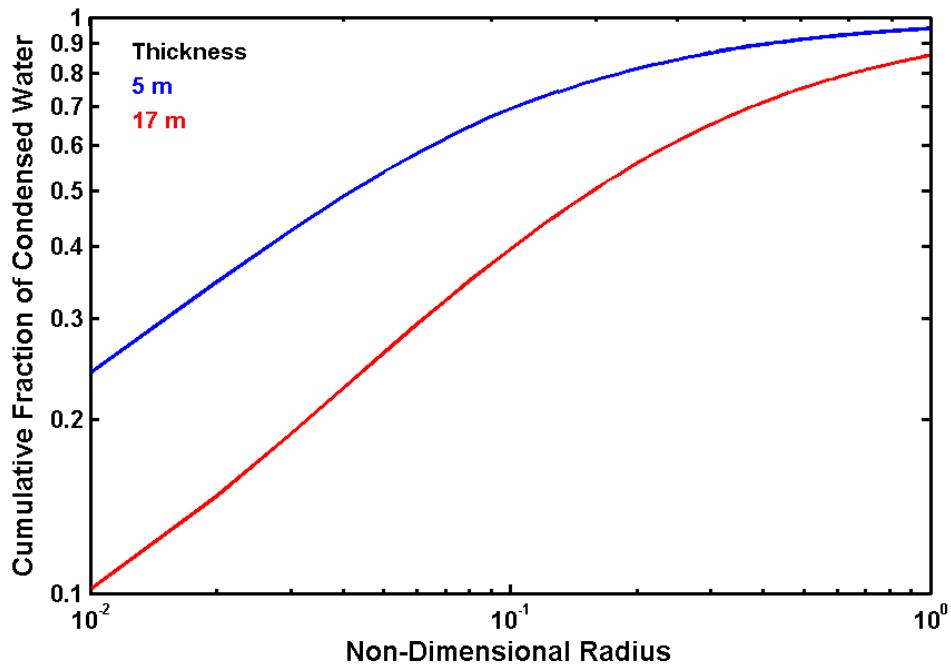


Figure 5-10. Radial Variation of Condensed Water for Different Dryout Thickness

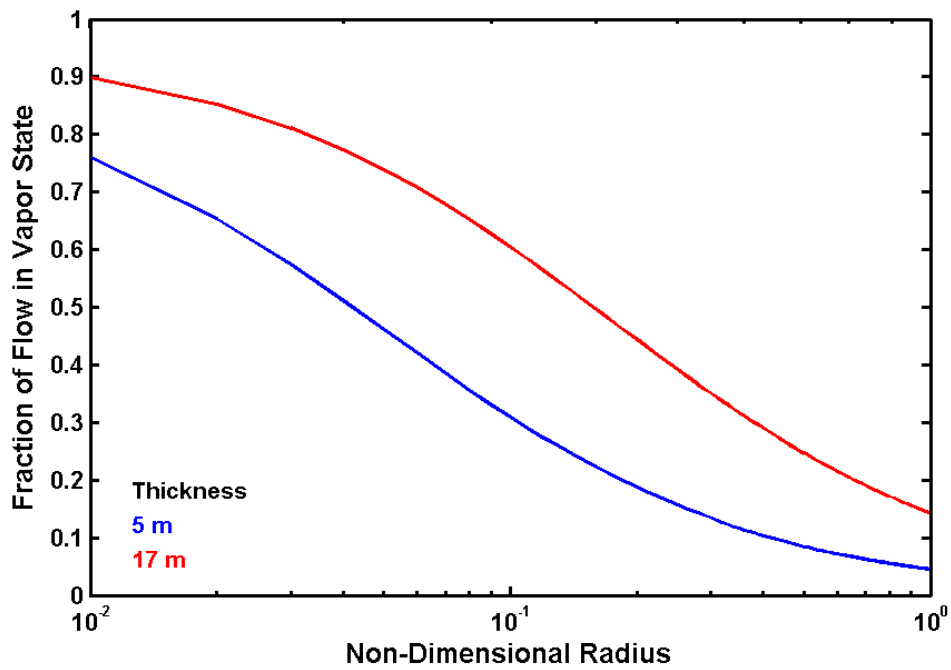


Figure 5-11. Radial Variation of Water Vapor for Different Dryout Thickness

6 THERMAL CONDUCTIVITY OF THE HOST ROCK

The Near-Field Environment module (NFENV)¹ in TPA Version 5.1 includes abstractions for heat transfer and temperature estimation on mountain and drift scales (Mohanty, et al., 2002a). The temperature at the drift wall is determined using a mountain-scale analytical heat conduction model. The model uses plate sources (finite width and finite length) to represent the heat generated from the line of waste packages in each drift. The general solution for temperature resulting from a plate source in a semi finite medium at any time and position [Mohanty, et al., 2002a, Eq. (5-1)] is a function of (i) time-dependent heat flux from decay of radioactive waste, (ii) thermal diffusivity of the host rock, (iii) representative effective thermal conductivity of the host rock (spatial and temporal average), (iv) width and length of the plate source representing waste packages emplaced along the drift, and (v) depth of the heat source. Superposition is used to combine the results from each drift to obtain a mountain-scale temperature distribution. Heat load (a design feature) and thermal conductivity of the host rock significantly influence the estimated waste package temperatures in the process-level sensitivity analyses (Mohanty, et al., 2002b). This section focuses on the representative host rock effective thermal conductivity values used in the NFENV module. Detailed process-level thermohydrological simulations were used to provide support for the distribution of host rock thermal conductivities in TPA Version 5.1.

The algorithm for calculating drift wall temperature in the NFENV module uses a representative effective thermal conductivity for the host rock. Thermal conductivity, however, is a function of saturation, which varies both spatially and temporally. The conduction-only analytical model uses a single effective (constant) thermal conductivity for the entire repository, whereas thermohydrological models use saturation-dependent thermal conductivity. In TPA Version 5.1, the spatial and temporal variations were captured by the lower- and upper-bound values that define the uniform distribution of representative effective thermal conductivity, and the distribution was based on the wet thermal conductivity values of the host rock. This approach of using wet thermal conductivity values for the uniform distribution is valid because the host rock is saturated (i.e., wet) at the mountain scale. The thermal perturbation caused by the emplaced waste will cause a region of dryout {approximately 10 m [32.81 ft]} only during the thermal period that is relatively short (a couple of thousand years) compared to the performance period. The distribution describing the thermal conductivity of the host rock also accounts for the effects of heterogeneity and the presence of lithophysae in host rock. Although there are four stratigraphic units intersected by the potential repository horizon, the thermal conductivity range used in TPA Version 5.1 was mostly based on the Tptpll, also called tsw35. This approach is appropriate because the tsw35 unit is the predominant unit at the repository horizon (Bechtel SAIC Company, LLC, 2004b).

Process-level simulations using a thermohydrological model, MULTIFLO (Lichtner and Seth, 1996; Painter, et al., 2001), have been conducted to refine the range for the thermal conductivity of the host rock, k , in TPA simulations. The results from a reference case MULTIFLO simulation in which k was varied as a function of space- and time-variant water saturations were compared to a set of MULTIFLO simulation results that assumed a constant k (in space and time) scaled to the thermal conductivity of the saturated host rock, k_{wet} . The latter is assumed to be

¹Near-Field Environment (NFENV) is referenced throughout this report, consequently the acronym NFENV will be used.

consistent with the conduction-only mountain-scale abstraction used to determine drift wall temperatures in TPA Version 5.1. The simulation results are shown in Figure 6-1.

In MULTIFLO simulations, $k_{dry} = 1.28 \text{ W/m-K}$ [$0.74 \text{ BTU/hr-ft-}^\circ\text{F}$] and $k_{wet} = 1.89 \text{ W/(m-K)}$ [$1.09 \text{ BTU/(hr-ft-}^\circ\text{F)}$], which were reported to be representative values for tsw35 in Bechtel SAIC Company (LLC, 2004a). The infiltration rates on the ground surface were chosen to be 5 mm/yr [0.19 in/yr] for 0–600 years, 14 mm/yr [0.55 in/yr] for 600–2,000 years, and 24 mm/yr [0.94 in/yr] after 2,000 years. These values are close to average percolation fluxes at the repository horizon used by Department of Energy, which were 6 mm/yr [0.24 in/yr] for 0–600 years, 16 mm/yr [0.63 in/yr] for 600–2,000 years, and 25 mm/yr [0.98 in/yr] after 2,000 years (Birkholzer, et al., 2004). In conduction-only simulations (that assume a constant k), the infiltration rate and pattern have no effect on drift-wall temperatures. The numerical results from the reference case with water saturation-dependent k (the blue curve in Figure 6-1) and the other simulations with a constant k (the red curves in Figure 6-1) were compared.

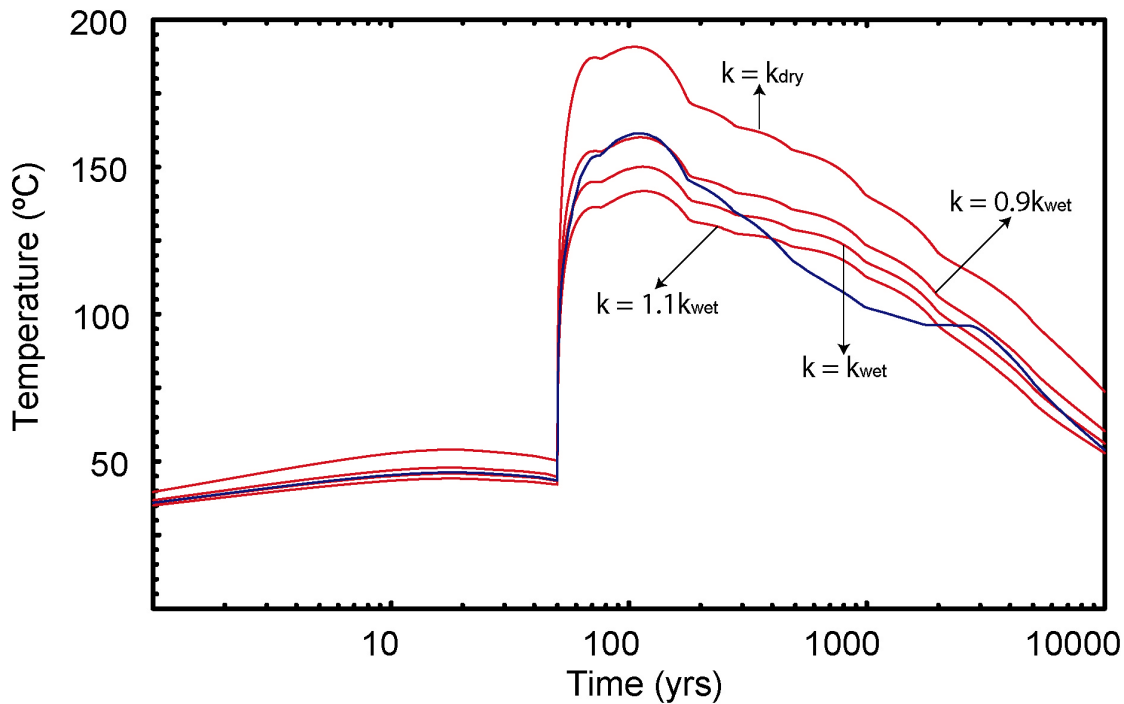


Figure 6-1. The Temperature at Drift Crown for an Intact Drift Obtained From MULTIFLO™ Simulations With Constant and Water Saturation Dependent Thermal Conductivity of the Host Rock. The Blue Curve Represents the MULTIFLO Result With the Thermal Conductivity of the Host Rock, k , That Varies With the Water Saturation. The Red Curves Correspond to the MULTIFLO Simulations With a Constant Thermal Conductivity of the Host Rock (Conduction-Only Simulations).

The peak temperatures at approximately 100 years reveal that the temperature obtained from the reference case overestimated the thermal conductivity for the dry host rock (k_{dry}).

A better match for the peak temperature from the reference case was achieved for $k = 0.9k_{wet}$. During the cooling period, the drift crown temperature was matched better with $k = 1.1 k_{wet}$. These results suggest that (i) it is appropriate to use k_{wet} values for the bulk thermal conductivity of the host rock at the mountain scale; (ii) the lower bound for k should be significantly greater than the thermal conductivity of the dry host rock, which was 1.20 W/(m-K) [$0.69 \text{ BTU/(hr-ft-}^\circ\text{F)}$]; and (iii) the upper bound for k should be slightly greater than the thermal conductivity of the saturated host rock, which was 2.13 W/(m-K) [$1.23 \text{ BTU/(hr-ft-}^\circ\text{F)}$].

Simulation results from the thermohydrological model that use saturation-dependent k values were compared with the TPA Version 5.1 simulation results that employ a constant k (in space and time) at the mountain scale. The main objective of this comparison is to provide upper and lower bounds for the (constant) effective thermal conductivity for the conduction-only abstraction in TPA Version 5.1. The results are shown in Figure 6-2.

Considering the differences in conduction-only heat transport and the water saturation-dependent heat transport processes, a perfect match between the simulation results from TPA Version 5.1 and MULTIFLO cannot be expected. However, the estimated temperature in the time-varying k shows consistent trends with the conduction-only abstraction. It is unclear in the performance assessment model whether higher or lower temperature estimates cause higher or lower release consequences due to competing effects. For example, release rates tend to be higher at higher temperatures, but are also delayed due to the longer time needed for seepage to form in the drifts. Therefore, for a performance assessment model, it is important to produce temperature estimates that are, on average, consistent with process-level model results. At longer time frames than 10,000 years, temperature computations tend to coincide.

Using a single value of thermal conductivity in TPA Version 5.1 to represent temperature history at the drift wall predicted by MULTIFLO can match either the peak temperature or pattern of thermal decay during the transition period (shown in Figure 6-2), but not both. The transition period is the duration where temperature significantly affects the chemistry and could lead to localized corrosion (Dunn, et al., 2005). The portion of the curve during the transition period was used to determine the representative value for thermal conductivity of the host rock. Based on the results shown in Figure 6-2, the thermal conductivity to be used in TPA Version 5.1 could range from 1.4 to 2.3 W/(m-K) [0.8 - $1.33 \text{ BTU/(hr-ft-}^\circ\text{F)}$], with a best calibrated value equal to 1.9 W/(m-K) [$1.10 \text{ BTU/(hr-ft-}^\circ\text{F)}$].

Implementation in TPA Version 5.1

The thermal conductivity of the host rock is defined by tpa.inp parameter ThermalConductivityofYMRock[W/(m-K)]. A distribution for this parameter ranging from 1.4 to 2.3 W/(m-K) [0.8 - $1.33 \text{ BTU/(hr-ft-}^\circ\text{F)}$] produces temperature estimates consistent with MULTIFLO simulations. The thermal conductivity could be sampled from a triangular distribution bounded by 1.4 and 2.3 W/(m-K) [0.8 - $1.33 \text{ BTU/(hr-ft-}^\circ\text{F)}$], with a mode of 1.956 W/(m-K) [$1.13 \text{ BTU/(hr-ft-}^\circ\text{F)}$]. The mode was selected to make the median of the distribution equal to 1.9 W/(m-K) [$1.10 \text{ BTU/(hr-ft-}^\circ\text{F)}$] which is the best fit value to the MULTIFLO data (Figure 6-2). The main effect of the drift-wall temperature in the TPA Version 5.1 computations

is to control the onset of aqueous conditions during corrosion and release computations. Lower temperature estimates are, in general, associated with an earlier onset of aqueous conditions at the waste package surface (establishment of these conditions is also dependent on drip shield performance). If the thermal conductivity is sampled only on the upper half of the thermal conductivity uncertainty distribution uniform distribution bounded by 1.9 and 2.3 W/(m-K) [1.10–1.33 BTU/(hr-ft-°F)], then temperatures are slightly underestimated resulting in earlier onset of aqueous conditions. This latter approach was adopted in TPA Version 5.1 uniform distribution ranging from 1.9 to 2.3 W/(m-K) [1.10–1.33 BTU/(hr-ft-°F)] to preferentially consider temperature estimates that would not result in underestimation of radionuclide releases in the first 10,000 years.

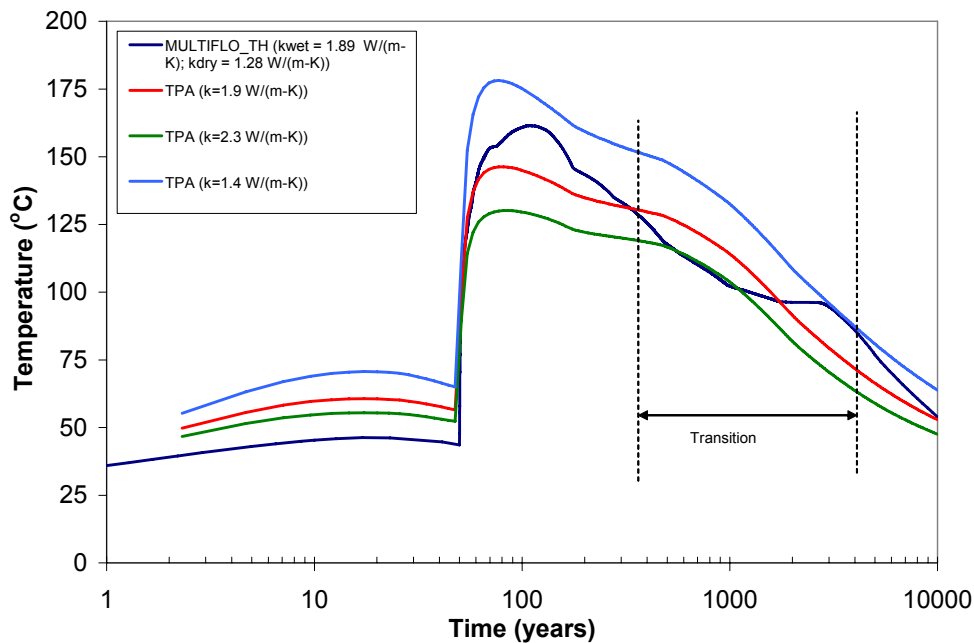


Figure 6-2. The Temperature at Drift Crown for an Intact Drift Obtained from TPA Version 5.1 With Constant Thermal Conductivity of the Host Rock. The Blue Curve Represents the MULTIFLO Result Where the Thermal Conductivity of the Host Rock Varies With the Water Saturation. The Other Curves Obtained from TPA Version 5.1 and use an Effective Thermal Conductivity Independent of Spatial and Temporal Variations in Water Saturations [$T^{\circ}\text{F} = 1.8 \times T^{\circ}\text{C} + 32$; $1 \text{ W}/(\text{m}\cdot\text{K}) = 0.577 \text{ BTU}/(\text{hr}\cdot\text{ft}\cdot^{\circ}\text{F})$].

7 SUMMARY

This report provides recent updates to the technical bases for several seepage factors used in Total Performance Assessment (TPA) Version 5.1 to account for changes in the deep percolation rate in the unsaturated fractured domain above the drift and across a part of the flow zone in the engineered barrier system (EBS). In the ambient period (no thermal perturbations), the seepage factors account for (i) mountain-scale flow convergence/divergence in the unsaturated fractured rock above the emplacement drifts, (ii) flow divergence in the immediate vicinity of the drift crown, and (iii) flow convergence/divergence across the rubble zone for the degraded (collapsed) drifts. In the thermal period, the effects of a thermally-driven dryout zone around the drifts on the deep percolation rates are considered. The seepage factors are simplified representations of fractured and unsaturated flows in the host rock and in the EBS. These factors affect the fraction of waste packages contacted by water, the onset of aqueous corrosion of waste packages, and dissolution, mobilization, and transport of radionuclides from failed waste packages.

In TPA Version 5.1, mountain-scale flow convergence in the host rock above the drift crown is correlated to the number of seep points on the drift ceiling. The greater the number of seep points at the drift ceiling, the wider the drainage (capture) zone of each seep point above the drift crown. The number of seep points on the drift crown is determined by the fraction of active fractures and the fracture spacing. The number of seep points on the drift ceiling is also used to determine the fraction of waste packages contacted by seepage. More seep points with closer spacing on the drift crown (i.e., less converged flow in the host rock above the drift crown) increase the number of waste packages contacted by seepage. Hence, there is an inverse correlation between the flow convergence in the host rock above the drift and the fraction of waste packages contacted by seepage. As the infiltration rate increases, more water would approach the drift crown, and hence more fractures would likely be active at the drift ceiling. This would lead to more waste packages being contacted by seepage. Hence, the infiltration rate at the ground surface is positively correlated to the fraction of waste packages contacted by seepage.

Infiltrating water approaching the drift crown can be diverted at the outer walls of the drift due to the capillary-barrier imposed by the drift opening. A fraction of water that seeps into a drift flows on the inner walls of the drift wall in films or rivulets based on the relative strength of the gravitational force exerted by the seepage and the capillary retention of the drift opening. The combined effects of these two processes on flow reduction at the drift crown were accounted for by a seepage factor defined in terms of a three-parameter sigmoidal curve. As the shift parameter of the sigmoidal curve decreases, the seepage fraction increases for a given percolation rate, and hence the total water volume diverted at the drift opening by capillarity and water diversion on inner walls of drift in films would decrease. This indicates that as the shift parameter decreases, water would converge more at seep points with less lateral diversion in the close vicinity of seep points. Hence, the shift parameter is negatively correlated to flow convergence above the drift crown.

In case of degraded (collapsed) drifts, the seepage should pass through the rubble zone before it contacts the EBS below. There are uncertainties in the size and shape distributions of rubble, and the connectivity of flow paths and the degree of flow convergence within the rubble zone. Therefore, the rubble zone is assumed not to change the flow rate in TPA Version 5.1. But, the model allows the users to incorporate temporal effects of rubble accumulation on the deep

percolation rate if detailed information on the nature and characterization of rubble, and the effect of rubble pile on the flow are available.

In TPA Version 5.1, thermal seepage through the dryout zone can occur when the potential penetration thickness of the condensed water exceeds the dryout zone thickness. A seepage threshold temperature is introduced in TPA Version 5.1 to prevent thermal seepage from breaching the dryout zone when the drift wall temperatures of intact drifts (or drip shield temperature of degraded drifts) exceeds the boiling temperature of water.

The report discusses preliminary results from exploratory quantitative analyses for the significance of the convective-diffusive flow cycle in the rubble zone after the thermal period, the effect of axial and radial transport of vapor inside the drift and in the rubble, flow and condensation of evaporated water above the dryout zone during the thermal period. The range of values for the thermal conductivity of the host rock was updated based on process level thermohydrological simulations and the report elucidated the technical bases for the changes.

A summary of range of values and distribution for TPA parameters including seepage factors and other seepage related parameters discussed at the Seepage Workshop, and correlations among the seepage factors are provided in Tables 7-1 and 7-2.

Table 7-1. TPA Parameters, Their Types, and Values		
Variable/Parameter Name	Type, Distribution	Bounds/Values
F_{wet}^{\dagger}	Constant	1.0
SubAreaWetFraction*	Sampled; Log-uniform	[0.25,1]
F_{ow}^{\dagger}	Constant	1.0
WastePackageFlowMultiplicationFactor*	Sampled; Log-uniform	[1,4]
F_{mult}^{\ddagger}		
AFmultCoefficient (of F_{mult})*	Constant	0.90
BFmultCoefficient (of F_{mult})*	Constant	0.5
X0FmultCoefficient (of F_{mult})*	Sampled; Triangular	[2.3, 3.4, 4.6]
SeepageThresholdT[C]*	Sampled; Triangular	[100.0, 105.0, 125.0]
ThermalConductivityofYMRock[W/(m-K)]*	Sampled; Uniform	[1.90, 2.30]
* tpa.inp parameter † auxiliary input parameter read from wpflow.def ‡ either computed by TPA Version 5.1 (default case) as described in Section 3.2 or read from an auxiliary input file (wpflow.def)		

Table 7-2. Correlations Between Seepage Factors	
Variables	Correlation Strength
SubAreaWetFraction vs. WastePackageFlowMultiplicationFactor	-0.99
SubAreaWetFraction vs. ArealAverageMeanAnnualInfiltrationAtStart[mm/yr]	0.7
WastePackageFlowMultiplicationFactor vs. ArealAverageMeanAnnualInfiltrationAtStart[mm/yr]	-0.7
X0FmultCoefficient vs. WastePackageFlowMultiplicationFactor	-0.9

8 REFERENCES

Albin, A.L., W.L. Singleton, T.C. Moyer, A.C. Lee, R.C. Lung, G.L.W. Eatman, and D.L. Barr. "Geology of the Main Drift—Station 28+00 to 55+00, Exploratory Studies Facility, Yucca Mountain Project, Yucca Mountain, Nevada." DOE Report DTN GS970208314224.005, Milestone Report SPG42AM3. Denver, Colorado: Bureau of Reclamation and U.S. Geological Survey. 1997.

Barr, D.L., T.C. Moyer, W.L. Singleton, A.L. Albin, R.C. Lung, A.C. Lee, S.C. Beason, and G.L.W. Eatman. "Geology of the North Ramp—Station 4+00 to 28+00, Exploratory Studies Facility, Yucca Mountain Project, Yucca Mountain, Nevada." DOE Report DTN GS960908314224.020. Denver, Colorado: Bureau of Reclamation and U.S. Geological Survey. 1996.

Beason, S.C., G.A. Turlington, R.C. Lung, G.L.W. Eatman, D. Ryter, and D.L. Barr. "Geology of the North Ramp—Station 0+60 to 4+00, Exploratory Studies Facility, Yucca Mountain Project, Yucca Mountain, Nevada." Denver, Colorado: Bureau of Reclamation and U.S. Geological Survey. 1996.

Bechtel SAIC Company, LLC. "Technical Basis Document 2: Unsaturated Zone Flow." Rev. 1. Las Vegas, Nevada: Bechtel SAIC Company, LLC. 2004

_____. "Drift Degradation Analyses." ANL–EBS–MD–000027. Rev. 03. Las Vegas, Nevada: Bechtel SAIC Company, LLC. 2004a.

_____. "Multiscale Thermohydrologic Model." ANL–EBS–MD–000049. Rev. 02. Las Vegas, Nevada: Bechtel SAIC Company, LLC. 2004b.

_____. "Thermal Testing Measurements Report." ANL–NBS–HS–000041. Rev. 00. Las Vegas, Nevada: Bechtel SAIC Company, LLC. 2002.

Bird, R., W. Stuart, and E. Lightfoot. *Transport Phenomena*. New York City, New York: John Wiley & Sons. 1960.

Birkholzer, J.T., S. Mukhopadhyay, and Y.W. Tsang. "Modeling Seepage into Heated Waste Emplacement Tunnels in Unsaturated Fractured Rock." *Vadose Zone Journal*. Vol. 3. pp. 819–836. 2004.

Dexter, A.R. "Heterogeneity of Unsaturated, Gravitational Flow of Water Through Beds of Large Particles." *U.S. Geological Survey Water Resources Research*. Vol. 29, No. 6. pp. 1,859–1,862. 1993.

Dunn, D.S., O. Pensado, Y.M. Pan, R.T. Pabalan, L. Yang, X. He, and K.T. Chang. "Passive and Localized Corrosion of Alloy 22—Modeling and Experiments." CNWRA 2005-02, San Antonio, Texas. 2005.

Eatman, G.L.W., W.L. Singleton, T.C. Moyer, D.L. Barr, A.L. Albin, R.C. Lung, and S.C. Beason. "Geology of the South Ramp—Station 55+00 to 78+77, Exploratory Studies Facility, Yucca

Mountain Project, Yucca Mountain, Nevada.” Denver, Colorado: Bureau of Reclamation and U.S. Geological Survey. 1997.

Fox, R.W., A.T. McDonald, and P.J. Pritchard. *Introduction to Fluid Mechanics*. Sixth Edition. Hoboken, New Jersey: John Wiley & Sons. 2005.

Green, R.T. and J.D. Prikryl. “Penetration of the Boiling Isotherm by Flow Down a Fracture.” *Proceedings of the Third International Symposium on Multiphase Flow*, Lyon, France, June 8–12, 1998. Lyon, France: Technomic Publishing Co. 1998.

Helton, J.C. and F.J. Davis. “Latin Hypercube Sampling and the Propagation of Uncertainty in Analyses of Complex Systems.” Chapter 5. Sandia Report SAND2001–0417. Albuquerque, New Mexico: Sandia National Laboratories, pp. 25–27. 2002.

Keenan, J.H., F.G. Keyes, P.G. Hill, and J.G. Moore. “Steam Tables: Thermodynamic Properties of Water, Including Vapor, Liquid, and Solid Phases.” Somerset, New Jersey: John Wiley & Sons. pp. 5.12. 1969.

Lichtner, P.C. and M.S. Seth. “Multiphase-Multicomponent Nonisothermal Reactive Transport in Partially Saturated Porous Media.” *Proceedings of the International Conference On Deep Geological Disposal Of Radioactive Waste*, Winnipeg, Manitoba, Canada, September 16–19, 1996. Toronto, Ontario, Canada: Canadian Nuclear Society. pp.133–142. 1996.

Lin, W., S.C. Blair, D. Wilder, S. Carlson, J. Wagoner, L. DeLoach, G. Danko, A.L. Ramirez, and K. Lee. “Large Block Test Final Report.” UCRL–ID–132246. Rev. 2. Livermore, California: Lawrence Livermore National Laboratory. TIC: 252918. 2001.

Liu, H.H. and G.S. Bodvarsson. “Constitutive Relations For Unsaturated Flow in a Fracture Network.” *Journal of Hydrology*. Vol. 252. pp.116–125. 2001.

Liu, H.H., R. Salve, J.S. Wang, G.S. Bodvarsson, and D. Hudson. “Field Investigation Into Unsaturated Flow and Transport in a Fault: Model Analyses.” *Journal of Contaminant Hydrology*. Vol. 74. pp. 39–59. 2004.

Liu, H.H., C.F. Ahlers, G.S. Bodvarsson, A.L. Flint, and W.B. Guertal. “Modeling Flow and Transport in Unsaturated Fractured Rock: An Evaluation of Continuum Approach.” *Journal of Contaminant Hydrology*. Vols. 62–63. pp. 73–178. 2003.

Liu, H.H., C. Doughty, and G.S. Bodvarsson. “An Active Fracture Model For Unsaturated Flow and Transport In Fractured Rocks.” *Water Resources Research*. Vol. 34. pp. 2,633–2,646. 1998.

Manepally, C., A. Sun, R. Fedors, and D. Farrell. “Drift-Scale Thermohydrological Process Modeling—In-Drift Heat Transfer and Drift Degradation.” CNWRA 2004-05. San Antonio, Texas: CNWRA. 2004.

Mohanty, S., T.J. McCartin, and D. Esh. “Total-system Performance Assessment (TPA) Version 4.0 Code: Module Descriptions and User’s Guide.” San Antonio, Texas: CNWRA. 2002a.

- Mohanty, S., R. Codell, J.M. Menchaca, R. Janetzke, M. Smith, P. LaPlante, M. Rahimi, and A. Lozano. "System-Level Performance Assessment of the Potential Repository at Yucca Mountain Using the TPA Version 4.1 Code." CNWRA 2002-05. Rev. 1. San Antonio, Texas: CNWRA. 2002b.
- Mongano, G.S., W.L. Singleton, T.C. Moyer, S.C. Beason, G.L.W. Eatman, A.L. Albin, and R.C. Lung. "Geology of the ECRB Cross-Drift—Exploratory Studies Facility, Yucca Mountain Project, Yucca Mountain, Nevada." SPG42GM3. Denver, Colorado: U.S. Geological Survey. 1999.
- Montan, D.N. and W.E. Bradkin. "Heater Test 1, Climax Stock Granite, Nevada." UCRL-53496. Livermore, California: Lawrence Livermore National Laboratory. 20p + appendices. 1984.
- Ofoegbu, G., R. Fedors, C. Grossman, S. Hsiung, L. Ibarra, C. Manepally, J. Myers, M. Nataraja, O. Pensado, K. Smart, and D. Wyrick. "Summary of Current Understanding Of Drift Degradation and Its Effects on Performance at a Potential Yucca Mountain Repository." CNWRA 2006-02. Rev. 1. San Antonio, Texas: CNWRA. 2006.
- Or, D., M. Tuller, and R. Fedors. "Seepage Into Drifts and Tunnels in Unsaturated Fractured Rock." *Water Resources Research*. Vol. 41, No. W05022. doi:10.1029/2004WR003689. 2005.
- Painter, S., P.C. Lichtner, and M.S. Seth. "MULTIFLO User's Manual MULTIFLO Version 1.5—Two Phase Nonisothermal Coupled Thermal-Hydrologic-Chemical Flow Simulator". San Antonio, Texas: CNWRA. 2001.
- Patrick, W. "Spent Fuel Test—Climax: An Evaluation Of The Technical Feasibility Of Geologic Storage Of Spent Nuclear Fuel In Granite. Final Report." UCRL-53702. Livermore, California: Lawrence Livermore National Laboratory. 297p. 1986.
- Phillips, O.M. "Infiltration of a Liquid Finger Down a Fracture Into a Superheated Rock." *Water Resources Research*. Vol. 32, No. 6. pp. 1,665–1,670. 1996.
- Salve, R. "Observations Of Preferential Flow During A Liquid Release Experiment In Fractured Welded Tuffs." *Water Resources Research*. Vol. 41, No. W09427. doi:10.1029/2004WR003570. 2005.
- Salve, R., H.H. Liu, P. Cook, and A. Czarnomski. "Unsaturated Flow and Transport Through a Fault Embedded in Fractured Welded Tuff." *Water Resources Research*. Vol. 40, No. W04210. doi:10.1029/2003WR002571. 2004.
- Salve, R., J.S.Y. Wang, and C. Doughty. "Liquid-Release Tests In Unsaturated Fractured Welded Tuffs: I. Field Investigations." *Journal of Hydrology*. Vol. 256. pp. 60–79. 2002.
- Seol, Y., H.H. Liu, and G.S. Bodvarsson. "Effects Of Dry Fractures On Matrix Diffusion In Unsaturated Fractured Rocks." *Geophysical Research Letters*. 1029/2002GL016118. 2003.
- Smart, K.J., D.Y. Wyrick, P.S. Landis, and D.J. Waiting. "Summary and Analysis of Subsurface Fracture Data From the Topopah Spring Tuff Upper Lithophysal, Middle Nonlithophysal, Lower

Lithophysal, and Lower Nonlithophysal Zones at Yucca Mountain, Nevada.” CNWRA 2005-04. San Antonio, Texas: CNWRA. 2006.

Stothoff, S., and G. Walter. “Long-Term-Average Infiltration at Yucca Mountain, Nevada: Million-Year Estimates. CNWRA 2007-003. Center for Nuclear Waste Regulatory Analyses, San Antonio. 2007.

Tokunaga, T.K., K.R. Olson, and J. Wan. “Infiltration Flux Distribution In Unsaturated Rock Deposits and Their Potential Implications for a Fractured Rock Formation.” *Geophysical Research Letters*. Vol. 32, No. L05405. doi:10.1029/2004GL022203. 2005.

Wyrick, D., R. Fedors, K. Smart, and R. McGinnis. “Trip Report: Field Examination of Fractures and Talus From Lithophysal Tuffs at a Rubble Analog Site, South End of Fran Ridge, Yucca Mountain, Nevada.” San Antonio, Texas: CNWRA. 2007.

Zhou, Q., R. Salve, H.H. Liu, J.S.Y. Wang, and D. Hudson. “Analysis Of A Mesoscale Infiltration and Water Seepage Test In Unsaturated Fractured Rock: Spatial Variabilities and Discrete Fracture Patterns. *Journal of Contaminant Hydrology*. Vol. 87. pp. 96–122. 2006.

Zimmerman, R.M., M.L. Blanford, J.F. Holland, R.L. Schuch, and W. Barrett. “Final Report: G-Tunnel Small-Diameter Heater Experiments.”SNL SAND84-2621, DE87-007361. Albuquerque, New Mexico: Sandia National Laboratories. December 1986.

Zimmerman, R.M., R.L. Schuch, D.S. Mason, M.L. Wilson, M.E. Hall, M.P. Board, R.P. Bellman, and M.P. Blanford. “Final Report: G-Tunnel Heated Block Experiment.” SNL SAND84-2620, DE86-011768 Albuquerque, New Mexico: Sandia National Laboratories. April 1986.